An Effective Method of Probe-calibration in Phase Resolved Near-field Scanning for EMI Application

Ji Zhang, Keong Kam, Jin Min, Victor Khilkevich,
David Pommerenke, *Senior Member, IEEE*, and Jun Fan, *Senior Member, IEEE*

***Abstract*—Near field scanning can be used to determine the far field emissions of electronic devices. In general, this requires phase resolved electric and magnetic near field data. To capture a broad frequency range relatively quickly, a multi-channel oscilloscope can be used for data capture. The phase relationship of the fields between different space-points and between the electric and the magnetic field needs to be known. Consequently, it is required to determine the complex-valued probe factor of the probe, cable and amplifier chain. This paper presents a fast and efficient calibration method which uses the same setup and instruments during calibration and measurement, and it allows for easy and economical integration of the calibration hardware and software into the scanning system. Known fields are created by a microstrip trace driven with a comb-generator. By referencing measured data to this known field, the probe factor is obtained over a broad frequency range by capturing one time-domain waveform.**

***Index Terms*— Electromagnetic interference (EMI), near field scanning, phase resolved, time domain measurement, probe calibration**

I. Introduction

ELECTROMAGNETIC models of ICs and modules are helpful for approximately predicting the emissions of a system or the intra-system coupling. One of the modeling methods is to calculate equivalent magnetic or/and electric current sources from near-field data above or around the under test (DUT) [1]-[4]. In this approach near-field scanning technique is used to capture sufficient field information. The scanned near-field data along the Huygens surface the emission source can be applied to source reconstruction far-field calculation [5][6].

Magnitude-only based electromagnetic-emission prediction has been reported, for example, in [7]. In principle only the magnetic or the electric field is needed; however, the most robust method is to capture both electric and magnetic field, including magnitude and phase [8]. The quality of scanned is usually determined by the properties of the probe (e.g. its sensitivity), the capability of suppressing unwanted components and the spatial resolution (if scanning was performed very close to the DUT). In most EMI near field scanning systems, a probe (or a set of probes) is located at a position close to the DUT. By moving the probe (or the DUT), a large set of field data is captured on a surface plane above the DUT [9][10][11]. Fig.1 shows the setup of a typical commercial scanning system. During the scanning measurements, cables and amplifiers are also needed for achieving connectivity and assuring a sufficient signal to noise ratio.

Fig.1. Near-field scanning platform [23]

A stable reference signal is required to resolve the phase of the signal captured by the probe. This signal can be directly taken from the active device or from a second field probe is fixed. In [12] and [13], two phase-measurement configurations are described: one method is to use vector network analyzer's (VNA's) external reference function; the other is to use a magnitude-only spectrum analyzer in conjunction with a power combiner (or hybrid coupler). However, either of these methods has its own drawback. Not the network analyzers have access to reference channel; moreover, the reference port often has a very limited dynamic range, especially for a mixture of narrowband and broadband signals. Using a spectrum analyzer and a hybrid requires at

This work was supported in part by the National Science Fundation.

J. Zhang, K. Keong, V. Khilkevich, D. Pommerenkce and J. Fan are with the Electromagnetic Compatibility Laboratory, Missouri University of Science and Technology, Rolla, MO 65401 USA (e-mail: jz7r9@mst.edu; kwkx8d@mst.edu; khilkevichv@mst.edu; davidjp@mst.edu; jfan@mst.edu).

J. Min is with the Amber Precision Instruments, Sunnyvale, CA 94085-1445 USA (e-mail: jinmin@amberpi.com).

three sweeps, each at different hybrid settings (such as sum difference). If the difference in magnitude between the reference and the probe signal is large, the difference between summation or a difference becomes very small, which leads to large errors in the phase determination, especially if signals not perfectly time invariant.

Another option is to scan the electromagnetic fields in time domain, as described in [10], [14] and [15]. Similarly to the scanning in frequency domain, a field probe is moved to different coordinates above the DUT; at each x-y coordinate, the outputs of field probe and reference probe are captured by an oscilloscope to collect a single-shot or averaged waveform. Later, all stored data is post-processed by Fast Fourier Transform (FFT) to provide phase-resolved field mapping. Our presented calibration method mainly serves for this time-domain scanning.

There are multiple advantages when applying time-domain scanning. With time-domain measurements, the knowledge of the phase is accessible without expensive instrument (i.e. VNA with specific functions) or complicated measurement procedure (i.e. three times of sweeping with spectrum analyzer). Another benefit of this approach is reduction of measurement time, due to its capability of capturing complete frequency ranges in one shot waveform. Moreover, it provides insight into the time dependence of signals, like occasionally appearing transient pulses. People need to notice that there is still drawbacks in time-domain scanning; one of the disadvantages is the low signal to noise ratio (S/N) compared with frequency domain measurements. In our work presented here, a low-noise amplifier will definitely be applied after the field-probe's output. Consequently, the S/N over the whole measurement system will be increased and the data's precision can be improved.

The captured voltages need to be converted to the electric and magnetic field above the DUT by using a frequency dependent and complex-valued probe factor.

For loop based magnetic field probes, a first order approximation of the induced voltage can be obtained using (1)

$$V(f) = j\omega\mu H(f) A_{eff} \tag{1}$$

Where, "f" is the frequency, "μ" is the permeability of air, "H" is the magnetic field strength in absence of the probe, and "A_{eff}" is the effective area of the loop. As it is difficult to deduce the effective area from the geometry of a shielded especially if uneven multi-turn loops are used, we consider methodology more as a plausibility check than a calibration method [9]. A further improvement is possible by including self-inductance which flattens the frequency response above a transition frequency determined by the low pass filter formed from the self-inductance and the load resistance [16][17]. However, this simple and quick method can only offer us a roughly estimated probe factor; it does not satisfy our requirement.

Plane-wave spectral domain theory allows for a better calibration, especially in cases in which the probe is strongly sensitive to unwanted field components [18]. The captured near-field data is expanded in the space-domain through Fourier-transformation, which allows obtaining a transfer-transfer-coefficient. However, in order to solve the linear equations, at least two different calibration structures (usually, two completely different PCBs) are required to offer linearly independent sets of near-field data. This significantly the complexity of the calibration method; thus, this technique not applied in our presented work.

Some existing techniques of probe calibration are based on estimating or calculating the complex antenna factor (CAF): the standard antenna method (SAM) calculates the CAF by theoretically estimate the antenna's characteristic (e.g. effective length, antenna height) [19]. The standard site method (SSM) performs the three-antenna measurement and calculates the CAF from obtained transmission coefficients [20]. However, the setup of three-antenna tests and the analysis of antenna properties may increase the overall complexity of the calibration procedure.

A simpler way is to obtain a probe factor by single point or distributed measurements of a known field using a network analyzer [9][21][22]. In principle, one can include the effect of amplifiers and cables by cascading their S-parameter representation [15]. However, we selected an oscilloscope for the phase-resolved scanning according to the multiple advantages of time-domain measurements. In order to avoid requiring another expensive instrument, we selected a time domain based calibration method which uses the same test setup during calibration as during measurements. The fixed setup can help reduce the chance of errors introduced by changing cables or amplifiers. A comb-generator is used to drive a microstrip trace and the probe under calibration is placed above this calibration board; this active source is able to cover a broad frequency range due to the narrow pulse signal. After FFT processing, the measured voltage is referenced to numerical simulated field data. This calibration procedure allows one to obtain the system probe factor, which includes all effects of the probe, cables and amplifiers and further electrical probe parameters. Here, we have a reasonable assumption that the probe can cause little back-scatter (the coupling impact onto the active source due to the presence of the probe) and have a sufficient suppression of unwanted field components (see Section III); otherwise, the distortion from the probe may need to be considered by a more sophisticated calibration mentioned in [6].

Our proposed time-domain calibration method is able to provide much more precise calibration results compared with "effective loop area" approach, while the complexity is significantly reduced than the techniques using plane-wave spectrum theory or three antennas test. As the calibration is performed with the whole scanning system, the obtained system probe factor can be directly utilized during the time-domain near field scanning. In our presented work, a single shot of waveform capturing can provide correct probe-factor in a wide frequency range from 10 MHz to 1 GHz.

The paper is structured as follows: Section II will give a introduction on the definition of probe factor and the detailed calibration methodology; the field probes (Electrical and

magnetic) are introduced in Section III; some essential probe parameters recovered during the calibration are reported in Section IV; the experimental results for calibrations and some potential challenges during practical implementation are discussed in Section V; then, a validation scan using this calibrated probe factor is presented in Section VI; finally, Section VII concludes our paper.

II. Determination of the Probe Factor

A. Probe Factor for Phase-resolved Time-domain Scanning

It is preferable to use the same setup for calibration and for the scanning measurements:

- The calibration structure can be integrated into the scanning system allowing a quick calibration prior to measurements
- The users do not have to characterize each elements of the setup (i.e. the cables, amplifiers and field-probes) individually; as the calibration is performed with the whole scanning system.
- The needed hardware is not expensive

The phase-resolved scanning setups are shown in Fig.2. As the final objective of performing near-field scanning is to obtain the electric and the magnetic field on a scanning surface, the captured voltage data on the multi-channel oscilloscope needs to be precisely converted to corresponding field strength. A complex-value parameter (or function) is required to describe this conversion, and this parameter (or function) is usually referred to as Probe Factor.

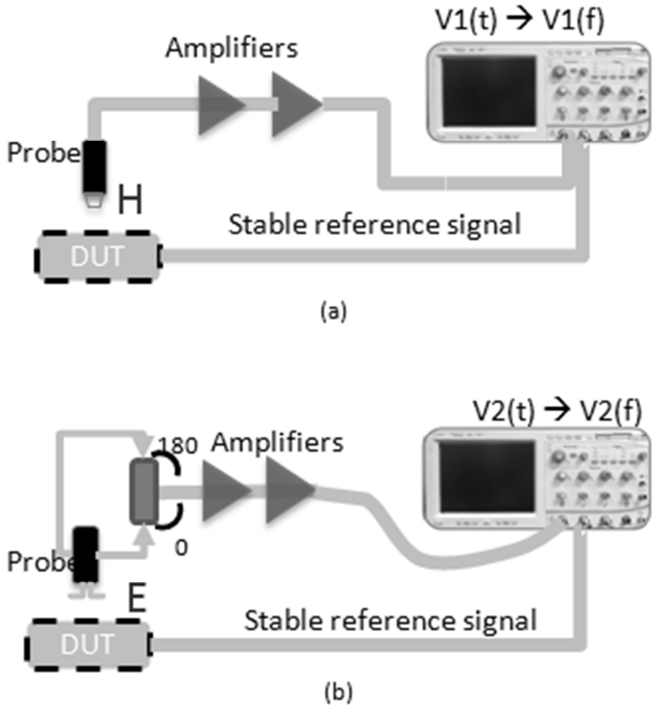

Fig.2. Setup of time-domain scanning
(a) H field scanning (b) E field scanning

Here the probe factor (PF) is defined as the complex valued, frequency dependent ratio of field strength at the location of probe (without the presence of this probe) to the voltage displayed on a multi-channel oscilloscope. It includes all the contributions from cables, hybrid couplers and amplifiers.

For the E-field probe the probe factor is defined as:

$$PF(f) \triangleq E(f)/V_{out}(f) \quad in\ unit\ of\ (V/m)/V \tag{2}$$

For the H-field probe the probe factor is defined as:

$$PF(f) \triangleq H(f)/V_{out}(f) \quad in\ unit\ of\ (A/m)/V \tag{3}$$

where E is the strength of the electrical field, H is the strength of the magnetic field, V_{out} is the measured voltage.

B. Methodology of Calibrating the Probe-factor

The probe factor is determined by referencing measured data to simulated field strengths, using the following steps:

1) Calculating the field strength above a microstrip trace.
2) Exciting a microstrip by a comb generator.
3) Placing the field probe above this calibration structure using the same cable, hybrid and amplifier setup as during near field scanning.
4) After converting to frequency domain, reference the measured voltage to the known field strength.
5) Calculate the frequency dependant probe factor.

In order to correctly capture the E and H field at one point, we need to make sure that the electrical center of E-field probe and H-field probe are placed at the same location above the trace. The vertical effective height of the E and H field probe can be précised determined respectively by observing the field-strength's null-point or slope when sweeping the probe across the trace, see Section IV.B. Regarding to the probe's horizontal effective center, the location error off to the side cannot be larger than 1 mm, as the probe's side thickness is around 1mm; this small shift will only impact the symmetry of the field-strength's null-point towards the left or right, but will not effect the field distribution a lot under the frequency of interest (e.g. 1 GHz).

We selected a terminated microstrip test board having 50 Ω impedance as a calibration structure. The field distribution above this microstrip calibration board can be obtained easily by approximate analytical solution or a full-wave simulation.

An active source is necessary to drive this microstrip test board and create the electromagnetic field. It can be a single frequency sine-wave generator or a comb-pulse generator.

The most straight forward method is to feed the 50 Ω trace with sine wave at a selected frequency. The drawback of this method is the long test-time. Only one frequency is available measure at each waveform capture, and the measurement to be repeated at a sufficiently large number of frequency sampling points. If the probe is located at one fixed position during the calibration this method would still be relatively as much shorter time records could be used; however, in order to obtain an estimation of the electrical-center of the probe (as

mentioned in Section IV.B), the probe is moved across the to take data at more than 50 positions for each frequency.

For the purpose of reducing calibration time and avoiding a costly RF signal generator, a comb generator based method, illustrated in Fig.3 and Fig.4, is a better choice. The comb generator provides pulse signals every 100 ns, which equals a frequency point sampling rate of 10 MHz allowing smooth interpolation. One waveform capture covers a broad frequency range due to the narrow pulse excitation signal; in our calibration case, the excitation signal from the comb generator is capable to cover a wide frequency range up to 1 GHz.

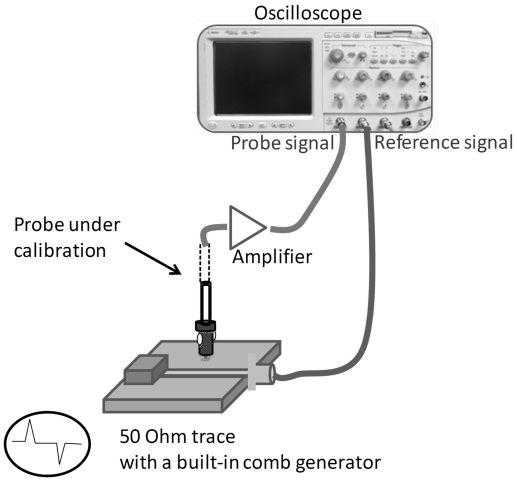

Fig.3. Setup of measuring the probe factor using a comb generator

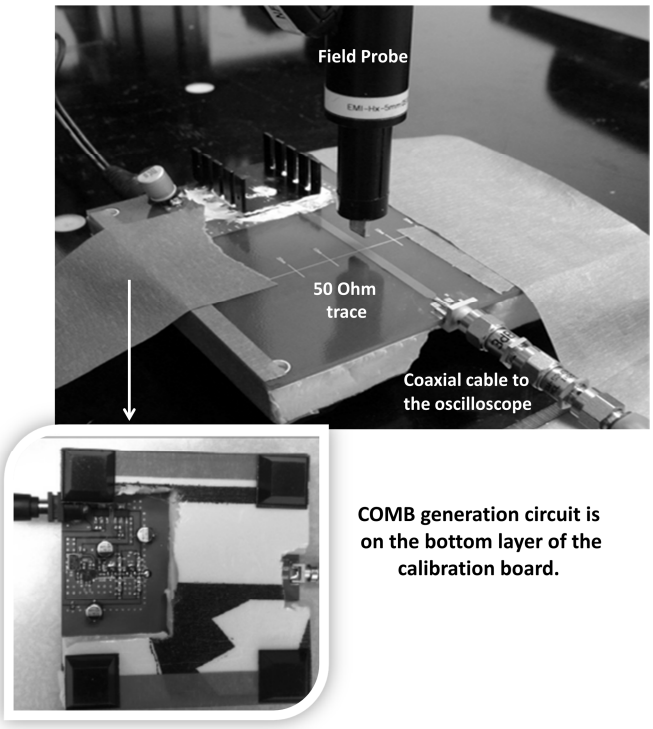

Fig.4. Photo of the calibration setup containing the comb generator

In the frequency range of interest (below 1 GHz), the microstrip can be considered as well matched to characteristic impedance (i.e. 50 Ohm) under this setup-condition; thus, a traveling-wave exists on the trace and the magnitude of voltage(or current) is the same along the whole trace. Then, field strength above the trace is a linear function of the trace voltage. However, this "well-matched" assumption may not be true for a higher operation frequency; and this could be one of the limitation factors for our method's frequency range. Under the assumption of "well matched microstrip", the simulated electric and the magnetic field above the trace (with CST Microwave Studio [24]) can be normalized to the trace voltage at each frequency point:

$$r_{EV}(\mathrm{f}) = {E_{simu}(\mathrm{f})}\Big/{\mathrm{V}_{\mathrm{trace-simu}}(\mathrm{f})} \quad (4)$$

$$r_{HV}(\mathrm{f}) = {H_{simu}(\mathrm{f})}\Big/{\mathrm{V}_{\mathrm{trace-simu}}(\mathrm{f})} \quad (5)$$

Where, $\mathrm{E_{simu}}$ and $\mathrm{H_{simu}}$ are the simulated field-strengths above the PCB; $\mathrm{V_{trace-simu}}$ is the amplitude of the trace used in simulation. The normalized field strength is needed for the next calibration steps.

Assuming that the cable for reference signal shown in Fig.3 and Fig.4 is of low-loss at frequencies of interest and that the input impedance of oscilloscope is well matched, the microstrip's voltage is precisely measured by the oscilloscope and then transformed to the frequency domain. The reference field strength above the trace is then obtained by multiplying the measured trace voltage with $\mathrm{r_{EV}}$ or $\mathrm{r_{HV}}$:

$$E_{ref}(f) = r_{EV}(f) \cdot V_{trace-mea}(f) \quad (6)$$

$$H_{ref}(f) = r_{HV}(f) \cdot V_{trace-mea}(f) \quad (7)$$

Where, $\mathrm{V_{trace-mea}}$ is the measured trace voltage.

After obtaining the reference field strengths the system probe factor can be finally calculated by:

$$PF_E(f) = {E_{ref}(f)}\Big/{V_{probe}(f)} \quad (8)$$

$$PF_H(f) = {H_{ref}(f)}\Big/{V_{probe}(f)} \quad (9)$$

Where, $\mathrm{V_{probe}}$ is the measured output voltage of the probe which includes all the effects of the cables and amplifiers.

III. Field Probes

To measure the tangential electrical field a probe utilizing two patches on opposite sides of a PCB is used (see Fig 5). An internal low noise amplifier provides gain and an external hybrid junction is used to obtain the differential signal suppressing common mode coupling. After further amplification the signal is connected to the oscilloscope.

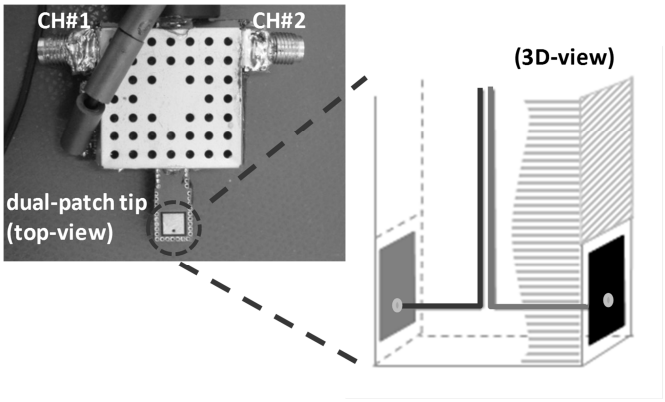

Fig 5: Photo of the electric-field probe

For capturing the magnetic field a shielded 5x5 mm loop is used, see Fig 6. The signal is further amplified and connected to the oscilloscope.

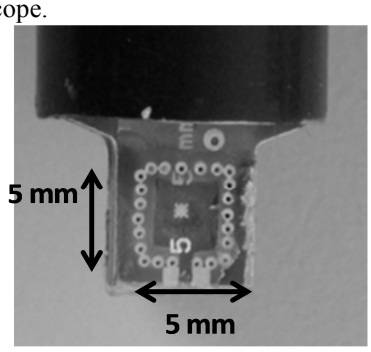

Fig 6: Photo of the magnetic-field probe

The system is mainly used up to 1 GHz. Both E-field and H-field probes show a resonance free transfer function up to 1 GHz. However, a field probe usually cannot perfectly suppressing the unwanted field component: an H-field loop probe may also collect a small amount of E-field component as the output; while a horizontal E-field patch probe may also capture some vertical E-field components, or even magnetic field components. In order to show our probes' capability on suppressing unwanted field components, the probe's frequency response was measured in a TEM cell with different probe rotation angles. Taking H field probe as an example, the loop probe was vertically placed into a TEM. Desirable field components (i.e. horizontal H-field) were obtained when the loop was perpendicular to the magnetic field; the loop with the orientation that was along with the magnetic field direction can only collect the unwanted field components. In Fig.7, the results prove that the probe is capable to suppress unwanted field components by more than 20dB within the frequency range of interest.

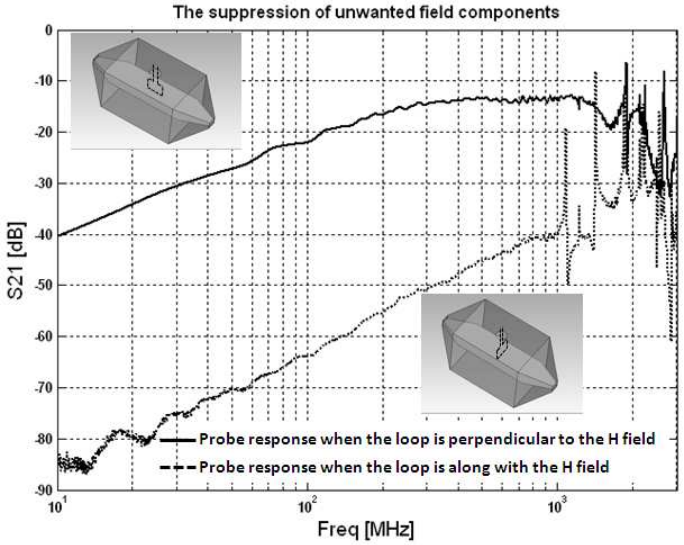

Fig.7: The suppression of unwanted field components (H field probe)

IV. Preparation for Calibration Measurements

A. Optimized probing position

The system probe factor includes the response of the field probe, cables and amplifiers. The probes are moved across the trace and the probe outputs are recorded in time domain at approximately 40 positions. At each position, the time-domain waveform was transformed to frequency spectrum, and this set of data is used to determine the optimized probing position for calibration and to identify the electrical center of the probe.

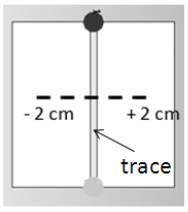

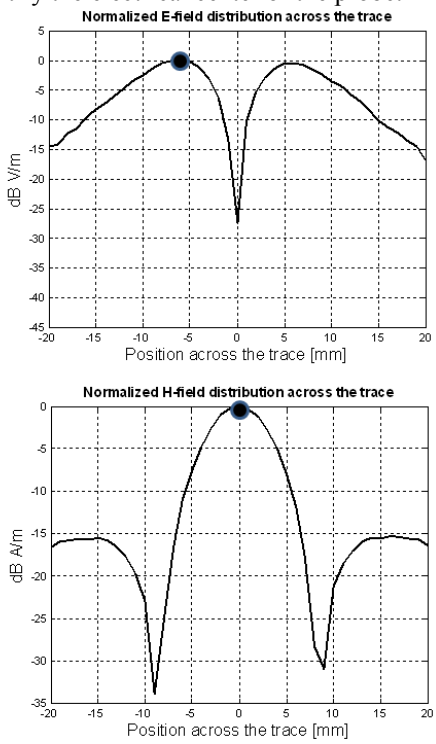

Fig 8: Horizontal E-field and horizontal H-field distribution across the trace

Fig 8 shows the distribution of the E and H field across the trace; here, the research frequency was selected but not necessary to be 200 MHz. The maximum of the horizontal E-E-field is to the side of the trace, while H-field has its

value right above the center of the trace. These positions are selected to calculate the probe factor.

B. Electrical center of the probe

Applying the measured tangential field strengths to a Huygens surface requires that both fields are measured in the same plane. This plane depends on the mechanical position of the probe and its electrical center (see Fig.9). The electrical center of the probe can be estimated by matching the simulated field distribution at different heights to the measured field distribution while crossing the trace [11]. The height which leads to the best match between the measured and the simulated distribution is taken as an approximation of the electrical height of the probe. This method matches the field distribution measured by a probe having a 5x5 mm loop to the simulated field at one height.

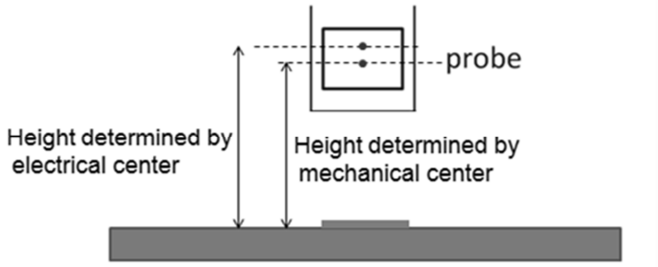

Fig.9. Electrical center and geometrical center

Fig.10 and Fig. 11 show the simulated magnetic/electrical field distribution across the trace for three different heights (6 mm, 8 mm and 10 mm) and one set of measured cross-sweep data (obtained in Section IV. A). For the horizontal magnetic field, the position of the nulls moves outwards with increasing height. In Fig.10, the 8 mm height simulated data matches the measured data best. Regarding to the horizontal electrical field, the cross-sweep distribution only shows a null directly above the trace which is not a function of height. However the position of the maximal signal, which is found to the left and to the right of the trace and the slope of the fall off are effected by the height, thus, they can be used to estimate the electrical center of the probe. As shown in Fig. 11, the 8 mm height simulated data indicates the best agreement with the measured horizontal E-field distribution. Consequently, we conclude that the estimated electrical height for both E and H field probe is 8 mm; while the mechanical center's height is actually 7 mm.

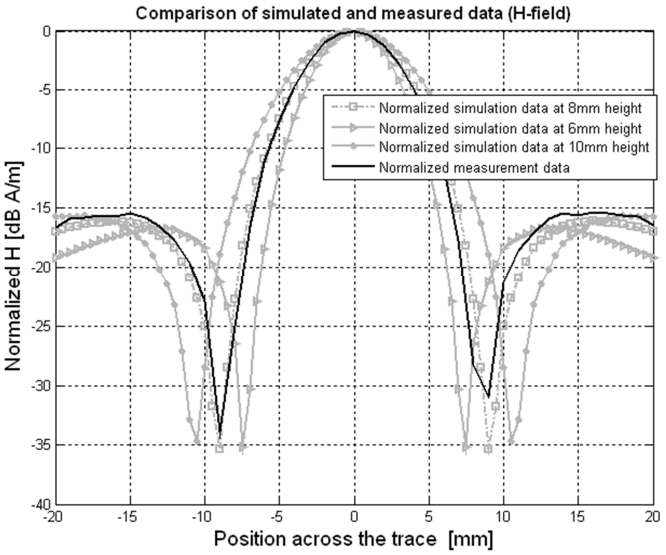

Fig.10. Tangential H-field strength across the trace at different heights (Simulation and measurement)

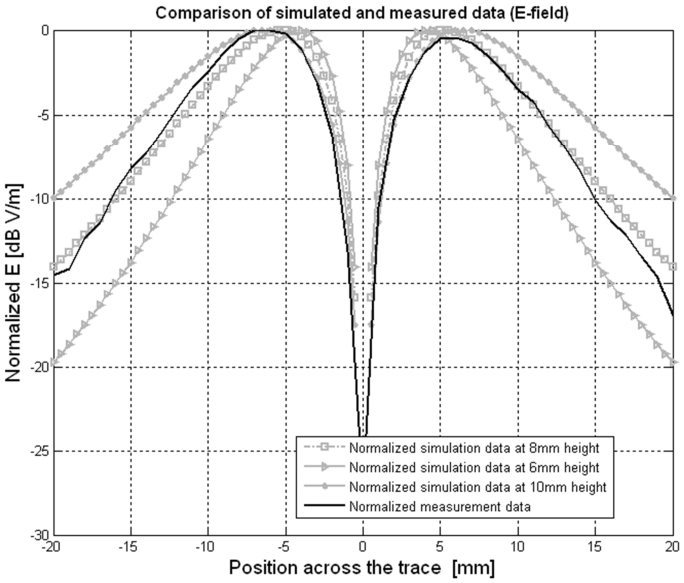

Fig. 11. Tangential E-field strength across the trace at different heights (Simulation and measurement)

V. Experimental Calibration Results

A. Probe signal and reference signal

As shown in Fig.3, two measured signals are necessary to determine the phase-resolved probe factor: the signal from the end of the microstrip, and the signal from the scanning probe. Fig.12 shows the periodic time domain waveforms. Because the probe signal and reference signal are recorded simultaneously our calibration method can recover the relative phase difference between E and H field. To determine the relative to the current that causes the fields, which is located directly underneath the probe, one would have to know the S-S-parameters between this point and the oscilloscope input. For Huygens surface based near field to far field there is no need to reference the phase to DUT currents; however, if in addition cable radiation is to be taken into account, and the cable radiation is captured using a current

probe, then all three phases (E, H and cable current) would be required.

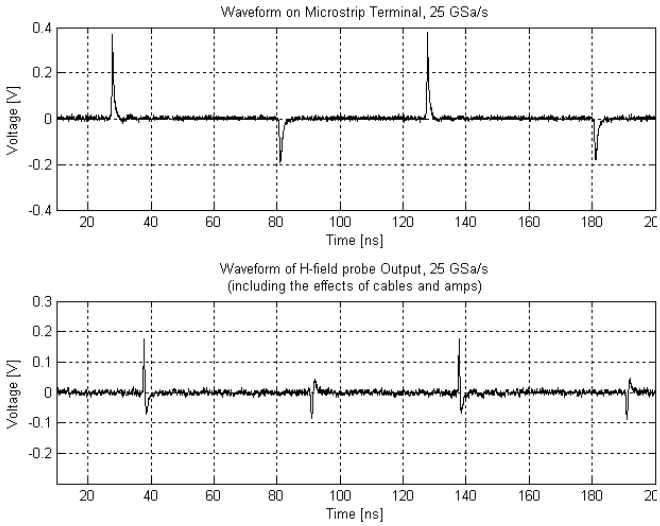

Fig.12. Measured microstrip-voltage (top) and field-probe output (bottom) during H field calibration

Before using the Fourier transformation to obtain the spectrum, a flat-top window function is first applied onto the measured time-domain data. The coefficients of the window function follow the equation:

$$w(n) = 0.2156 - 0.416\cos\left(\frac{2\pi n}{N}\right) + 0.2781\cos\left(\frac{4\pi n}{N}\right) - 0.0836\cos\left(\frac{6\pi n}{N}\right) + 0.0069\cos\left(\frac{8\pi n}{N}\right); \quad (10)$$

where, N is the total data length, n is the index of data sample.

The comb-generator output has both positive and negative pulses (see Fig.12), which causes odd and even harmonics of the 10 MHz signal to be of different amplitude, as shown in Fig.13. The probe's out signal and reference signal in frequency domain are then ready for further calculation to obtain the phase-resolved probe factor, according to equation (8) and equation (9). The probe's frequency response rolls off towards low frequencies, as a consequence of the derivative operation of magnetic fields. Thus, the sensitivity of the probe itself is low at low frequencies. However, as long as the calibration procedure is able to recover a signal of sufficient strength (e.g. by applying low noise amplifiers, or choose a location where field strength is relatively large), our presented calibration will be able to determine the probe factor correctly. In our work, we have managed to obtain the signal that is outstanding from the noise floor by at least 10 to 20 dB (even at 10 MHz).

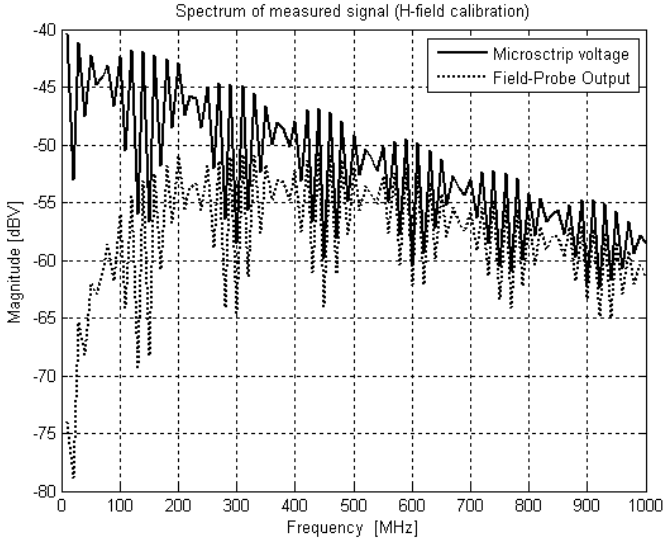

Fig.13. Spectrum of the H-field probe output and the microstrip output signal plotting only data points at N x 10 MHz

B. *Challenges during the calibration*

First, the effect of reflections between the probe and the first amplifier need to be considered (see Fig.14). The probe's reflection coefficient is close to 1, and typically low noise amplifiers also do not offer a good input match. Thus, multiple reflections will cause an undulation of the probe factor. These do not effect the measurements, as they are included within the probe factor.

The second difficulty is a direct result of using a comb generator. A comb generator distributes its energy over many harmonics which can lead to signal to noise ratio problems especially at high frequencies where the spectral density drops. Using a strong comb generator will improve the signal to noise ratio. However, during the calibration and measurements, two or three stages of amplifiers are usually applied after the probe output, with around 20 dB gain for each stage. In this case, the large crest factor from a strong comb generator can cause small non-linearity during calibration if the second amplifier is driven out of its linear range. This leads to incorrect probe factors, as this non-linearity is only present during the calibration. One needs to limit the output power of the comb generator by reducing the gain of integrated amplifiers in comb-signal generation circuit; removing any amplifier that follows the field probe during calibration violates the condition of having the same setup during calibration and near field measurements. The underlying assumption of the calibration is the linearity of the probing system, including amplifiers and the oscilloscopes; consequently, the signal levels have to be kept low enough to avoid nonlinearity. An illustration of a correct field probe factor and the probe factor distorted by non-linearity is shown in Fig.15; the correct E-field probe factor is also presented (see Fig 16). The upper-frequency limitation of a calibration system is effected by several factors: characteristics of the field probe, the cable, the amplifier and the comb-generator. In our case, we can achieve a correct and useful probe factor up to 1 GHz.

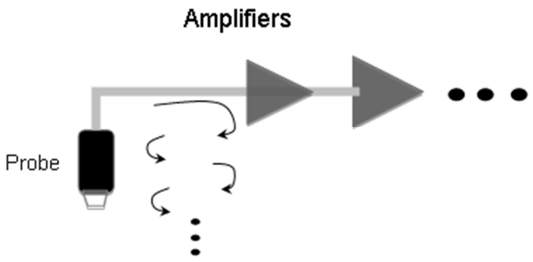

Fig.14. Multiple reflections due to mis-match of 1st stage amplifier

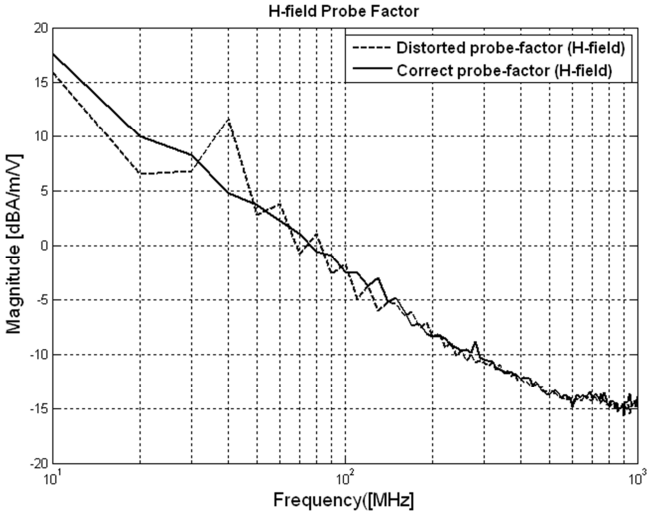

Fig.15. H-field probe factor (comparing correct one with the distorted one)

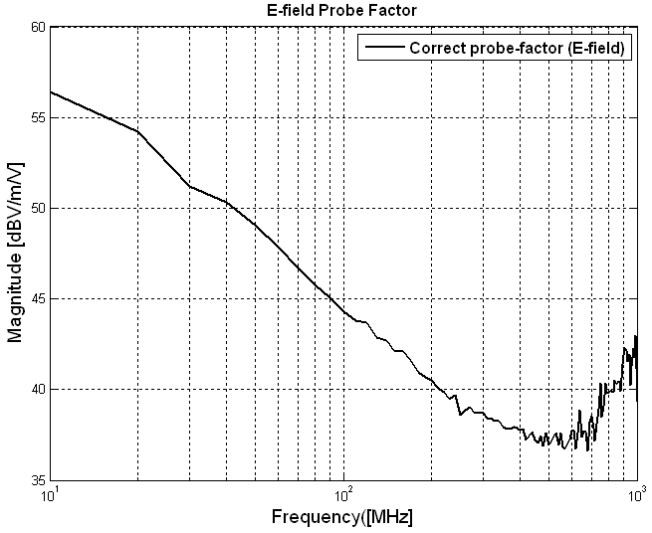

Fig 16: E-field probe factor (the correct one)

VI. Validation Based on Calibrated Probe Factor

A. Effective loop area

Based on the calculated probe factor, the effective loop area of the H-field probe can be estimated by equation (1) and (3) as a sanity check.

Estimating the effective area of the H-field probe led to $22\,mm^2$ at 80 MHz. As equation (1) does not take the integrating effect of the self-inductance into account, one would observe a decrease of the effective area above the transition frequency; however, below this frequency, as long the probe factor shows a 20dB/dec rise, the effective area will not be a function of frequency. The physical loop area is $25\,\mathrm{mm}^2$ as shown in Fig 6. The difference is small, supporting the correctness of the methodology.

B. Verification by TEM cell measurements

A more precise verification method is to calculate the probe factor in TEM cell and then compare it with the result obtained from our proposed calibration approach. In TEM cell, the electromagnetic fields are derivable based on equation (11) and equation (12)

$$E = V_{in}/d_{TEMcell} \quad (11)$$

$$H = E/\eta = V_{in}/(d_{TEMcell} \cdot \eta) \quad (12)$$

where, $d_{TEMcell}$ is the distance between septum and out-out-conductor, η is the wave-impedance in the air, V_{in} is the incident voltage of TEM cell. By using network analyzer to measure the ratio of field probe's output voltage to the input voltage of TEM cell, the probe factor can be expressed as a function of S21 parameter:

$$E\ field\ probe\text{:}\ PF = 1/(S21 \cdot d_{TEMcell}) \quad (13)$$

$$H\ field\ probe\text{:}\ PF = 1/(S21 \cdot d_{TEMcell} \cdot \eta) \quad (14)$$

Table I shows an illustration of comparing our proposed calibration results with the TEM cell calibration results at several frequency points. The probing system, including field probes, cables and amplifiers, for these two types of calibration tests are exactly the same. The comparison shows that the difference from these two completely different methods is less than 1 dBc.

TABLE I
COMPARISON OF CALIBRATED PROBE FACTORS (Magnitude: dB)

	10 MHz	30 MHz	300 MHz	500MHz
Proposed method	28.43	18.38	1.626	0.6847
TEM cell method	27.26	17.42	1.161	0.7261

C. Near-field scanning on validation device

The correctness of the probe factor was further verified by comparing simulated near fields to the scanned near fields. Here the test structure was a microstrip having a copper patch, as shown in Fig.17. The excitation signal generator was integrated on the bottom layer of the board; the ground plane at the bottom of the board was well connected and supported by an aluminum shielding box.

After performing the comb-generator based calibration, the time domain near-field scanning was performed above this device, and the captured voltage data was converted to field strength based on the calibrated probe factor. The horizontal E-field mapping from processed measurement data and full-full-wave simulation data are compared in Fig.18 and Fig.21, at frequencies of 200 MHz and 900 MHz respectively; similarly, in Fig.23, the horizontal H field pattern at 900 MHz are plotted. All of the field-mapping comparisons show a good agreement between the measurements (after applying calibrated probe-factor) and simulations. Furthermore, Fig.19 and Fig.22 show the field distribution (both magnitude and phase) along a cut-line across the trace: the processed

measurement field magnitude are close to the simulated field strength; the phase offset is a result of referencing the scanned-data's phase to the oscilloscope input, rather than directly to the current/voltage on the trace. As mentioned above, this constant phase offset is impacted by the reference-signal cable; but it does not effect the NF-FF transformation, as the same referencing is used for both E and H field.

In order to quantify the relative error between measured and simulated field, we define the relative error as the following equation:

$$RE = |E_{t.sim} - E_{t.mea}|/|E_{t.sim}|$$

Where, $E_{t.sim}$ is the simulated horizontal E field strength, $E_{t.mea}$ is the measured horizontal E field strength after calibrated probe factor. Taking the Ex field at 200 MHz for example, in Fig.20, the distribution of relative error was plotted, while the error value was clamped up to 100 percent. the region where field strength level is relatively small (i.e. 20 dB lower than the maximum value), a small measurement could also cause huge relative error according to equation However, this type of large relative error does not have much impact on the near- field to far- field transformation or source reconstruction, due to the small field strength. From Fig.20 people can notice that the "large error region" is always associated with the "small signal region"; besides this area, the relative error between measurements and simulation is usually lower than 20%.

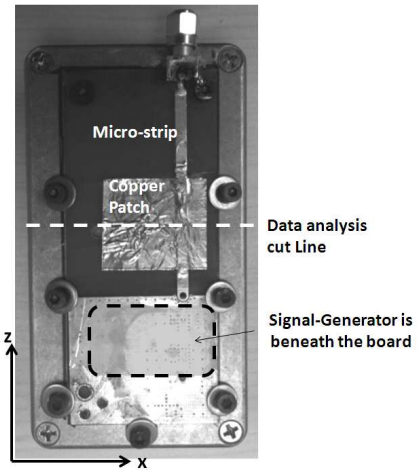

Fig.17. Device for scanning validation

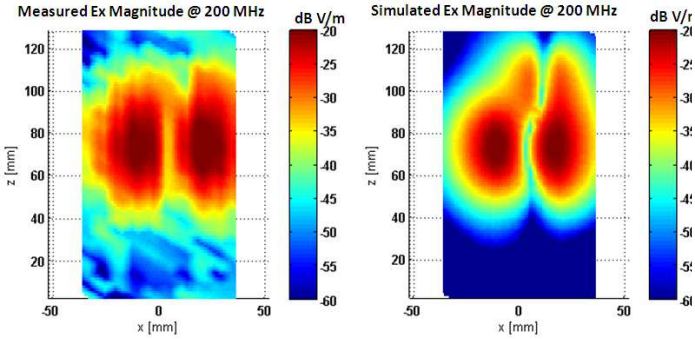

Fig.18. Simulated and measured Ex field mapping @ 200 MHz

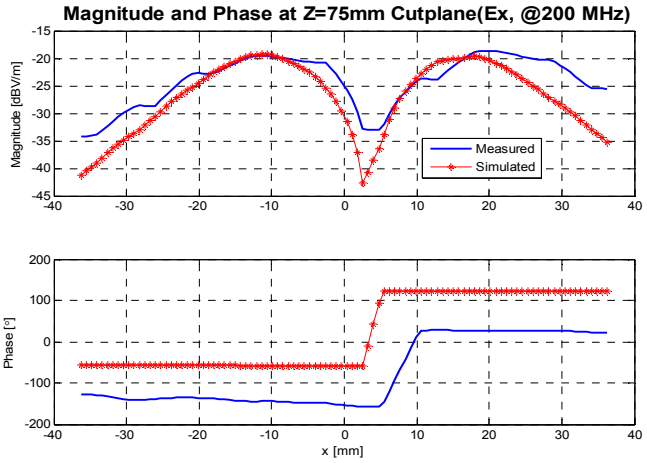

Fig.19. Ex field across the cut-line z = 75 mm (@ 200 MHz)

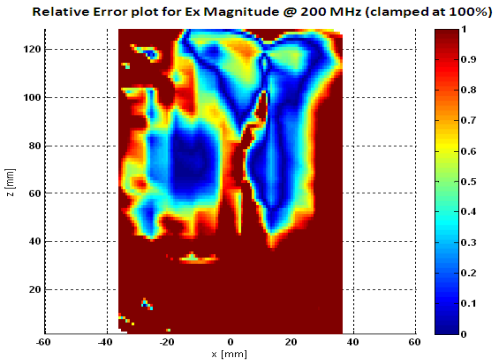

Fig.20. Relative error between simulated and measured field mapping

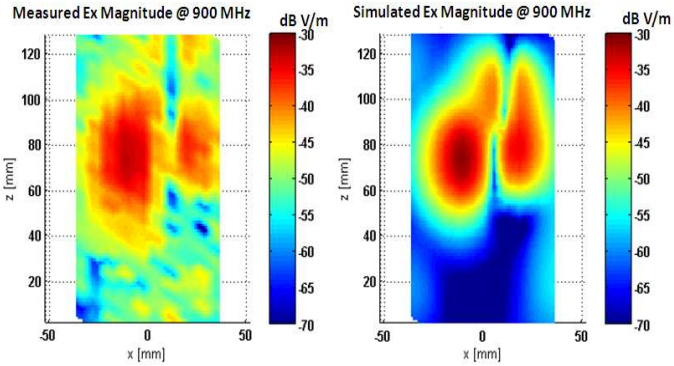

Fig.21. Simulated and measured Ex field mapping @ 900 MHz

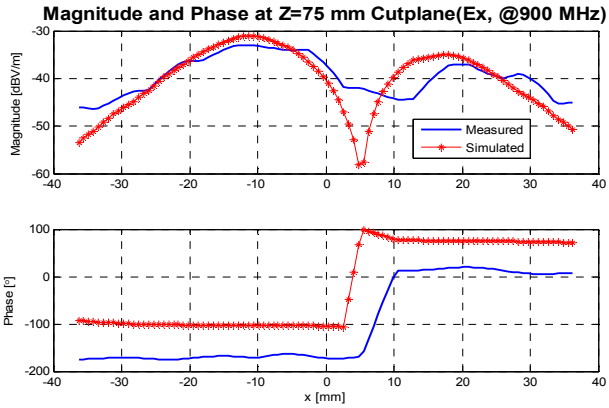

Fig.22. Ex field across the cut-line z = 75 mm (@ 900 MHz)

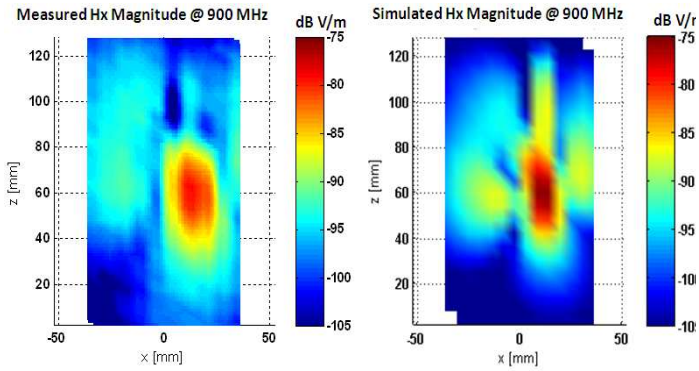

Fig.23. Simulated and measured Hx field mapping @ 900 MHz

VII. CONCLUSION

We report a calibration method for E-field and H-field probes having phase resolved near field scanning for near to far field transformation in mind. The calibration method uses a comb generator driven trace and an oscilloscope to achieve broadband magnitude and phase capture. The method uses the same test setup during calibration and time domain measurements reducing errors caused by cable or amplifier changes and it allows referencing the phase of the E-field to the phase of the H-field, an essential property needed for the far field transformation. For determining the probe factor, the measured field is compared to a numerically calculated field above the trace, allowing determining the probe factor and the electrical center of the probe. The investigations have shown that using a comb generator allows fast probe calibration which can be smoothly integrated into the time domain based scanning system; however, care must be taken to avoid non linear effects in the amplifiers caused by the large crest factor of the comb generator. On the other hand, the DUT under scanned does not have to a linear device, some digital device such as cell phones or motherboards have been scanned; of course, the scanned results are only valid for the working conditions which the devices were operated on.

REFERENCES

[1] P. Fernández López, C. Arcambal, D. Baudry, S. Verdeyme, B. Mazari, "Simple Electromagnetic Modeling Procedure: From Near-Field Measurements to Commercial Electromagnetic Simulation Tool," *IEEE Trans. Instrum. and Meas.,* vol. 59, no. 12, pp. 3111-3121, Dec. 2010.

[2] P. Petre and T. K. Sarkar, "Planar near-field to far-field transformation using an equivalent magnetic current approach," *IEEE Trans. AntennasPropag*., vol. 40, no. 11, pp1348-1355, Nov. 1992.

[3] A. Taaghol and T.K. Sarkar, "Near-field to near/far-field transformation for arbitrary near-field geometry utilizing an equivalent magnetic current," *IEEE Trans. Electromagn. Compat*., vol. 38, no.3, pp. 536-542, Aug. 1996.

[4] T. K. Sarkar and A. Taaghol, "Near-field to near/far field transformation for arbitrary near-field geometry utilizing an equivalent electric current and MoM," *IEEE Trans. Electromagn. Compat.,* vol. 47, no.3, pp .566-573, Mar. 1999.

[5] Y. Alvarez, M. Rodriguez, F. Las-Heras, and M.Hermando, "On the use of the source reconstructing method for estimating radiated EMI in electronic circuits," *IEEE Trans. Instrum. and Meas.,* vol. 59, no. 12, pp. 3174-3183, Dec. 2010.

[6] H. Weng, D. G. Beetner, R. E. DuBroff, "Prediction of radiated emissions using near field measurements," *IEEE Trans, Electromagn. Compat.,* vol. 53, no. 4, pp. 891-899, Nov. 2011.

[7] B. Deutschmann, H. Pitsch, and G. Langer, "Near field measurements to predict the electromagnetic emission of integrated circuits," *5th International Workshop on Electromagnetic Compatibility of Integrated Circuits*, Nov. 2005, Munich, Germany

[8] D. Baudry, A. Louis, B. Mazari, "Overview of emission and susceptibility investigation and modeling with near-field measurements," *The 2008 General Assembly of the International Union of Radio Science (Union Radio Scientific International -URSI),* 2008

[9] D. Baudry, C. Arcambal, A. Louis, B. Mazari and P. Eudeline, "Applications of the Near-Field Techniques in EMC Investigations", *IEEE Trans. Electromagn. Compat*., vol. 49, no. 3, pp. 485-493, August 2007.

[10] T. Mager, C. Reinhold, C. Hedayat, T. Gessner, "Near Field Scanner in Time and Frequency Domain," *MST News (2009)* 1, pp.40-41

[11] C. Avram, G. Gavrila, J. Tao, "Characterization of Miniature Near Field Probes for IC's Radiation Measurements," *8th int Conf on Communications*, 10-12 June 2010, Bucharest, pp. 275-278

[12] Y. Vives-Gilabert, C. Arcambal, A. Louis; F. de Daran, P. Eudeline, B. Mazari, "Modeling Magnetic Radiations of Electronic Circuits Using Near-Field Scanning Method," *IEEE Trans. Electromagn Compat*., Vol: 49 , Issue:2, 2007, pp. 391-400.

[13] X. Tong, "Simplified Equivalent Modelling of Electromagnetic Emissions from Printed Circuit Boards," *Thesis submitted to the University of Nottingham for the degree of Doctor of Philosophy*, May 2010.

[14] T. Ordas, M. Lisart, E. Sicard, P. Maurine, L. Torres, "Near-field Mapping System to Scan in Time Domain the Magnetic Emissions of Integrated Circuits," *PATMOS'08: International Workshop on Power and Timing Modeling Optimization and Simulation*, 2008

[15] T. Stadtler, L. Eiflter, J. L. ter Haseborg , "Double Probe Near Field Scanner, a New Device for Measurements in Time Domain," *Electromagnetic Compatibility, 2003 IEEE International Symposium on*, 18-22 Aug. 2003, pp 86 -90.

[16] N. Uddin, M. Spang, T. Mager, A. Thiede, "Integrated Active Sensor for Near-Field Scanning," *Theoretical Engineering (*ISTET), 2009 XV International Symposium on, 22-24 June 2009, pp 1-5.

[17] S. Jarrix, T. Dubois, R. Adam, P. Nouvel, B. Azais and D. Gasquet, "Probe Characterization for Electromagnetic Near-Field Studies, " *IEEE Trans. Instrum. and Meas,* Feb. 2010, vol. 59, pp 292 – 300.

[18] M. Spang, T. Stoeckel, G. Schubert and M. Albach, "Application of probes with multiple outputs on probe-compensated EMC near-field measurements," *Industrial Technology* (ICIT), 2010 IEEE International Conference on, 14-17 March 2010, pp 188-193.

[19] K. Fuji, S. Harada, A. Sugiura, Y. Matsumoto, Y. Yamanaka, "An Estimation Method for the Free-Space Antenna Factor of VHF EMI Antennas," *IEEE Transactions on Electromagnetic Compatibility*, Vol. 47, No. 3, August 2005, pp. 627-634.

[20] S. Ishgami, H. Ida, T. Iwasaki, "Measurements of Complex Antenna Factor by the Near-Field 3-Antenna Method," IEEE Transactions on Electromagnetic Compatibility, Vol. 38, No. 3, August 1996, pp. 424-432.

[21] A. Tankielun, P. Kralicek, U. Keller, E. Sicard, B. Vrignon, "Influence of Core Optimisation and Activity for Electromagnetic Near-Field and Conducted Emissions of CESAME Test Chip," *Proc. EMC Compo 2004 conference*, Angers, France, April 2004, pp. 95-100

[22] IEC 61967-3, "Integrated circuits - Measurement of electromagnetic emissions, 150 KHz to 1 GHz - Part 3: Measurement of radiated emissions - Surface scan method, Ed. 1", www.iec.ch, 2005

[23] (2011) The API website: http://www.amberpi.com

[24] CST Microwave Studio 2011: http://www.cst.com/